Available online at www.sciencedirect.com
SCIENCE DIRECT®
Minerals Engineering 18 (2005) 1164–1172
MINERALS ENGINEERING
This article is also available online at: www.elsevier.com/locate/mineng

Bubble size distribution in laboratory scale flotation cells

R.A. Grau *, K. Heiskanen

Helsinki University of Technology, P.O. Box 6200, 02015 TKK, Finland

Received 7 April 2005; accepted 17 June 2005
Available online 18 August 2005

Abstract

Bubble size was measured in two lab scale cells using the HUT bubble size analyzer. The influence of operating conditions on bubble size was investigated. The Sauter mean bubble size was found to vary over the range of 1.2–2.9 mm. The experimental bubble size distributions were satisfactorily represented by the upper-limit distributions.

The frothers were found to have a profound impact on bubble size. It seems that frothers not only prevent bubble coalescence, but they also, affect the bubble break-up process. The air flow rate was also found to have a strong influence on bubble size. The Sauter mean bubble diameter increased as the air flow rate increased. The Sauter mean bubble diameter was found to decrease with increasing impeller speed. The addition of quartz on the other hand was found to increase the size of bubbles, this effect was more evident at solid concentration exceeding 20% (kg/kg). The size of bubbles generated with the multi-mix and free-flow mechanisms were different at similar operating conditions, in a non-coalescing environment. The free-flow design generated broader bubble size distributions than the multi-mix mechanism.

Keywords: Flotation bubbles; Flotation frothers; Flotation machines

1. Introduction

Bubble size (d_b) is an important parameter, which defines along with gas hold-up and gas velocity how efficiently the air is dispersed in a flotation cell. Ahmed and Jameson (1985) assumed that the removal of particles can be described by a first-order rate equation. They found that bubble size has a strong influence on the flotation rate constant (k), recognizing also that the flotation rate constant is a complex function of the particle properties and the hydrodynamic conditions in the cell. Yoon (2000) derived from first principles that the first-order kinetic constant varies as d_b^{-3} at quiescent conditions. However, under turbulent conditions, as the case in mechanical cells, it is known that the flotation rate constant is less influenced by bubble size (Heiskanen, 2000). The flotation rate constant is expected to approximately vary as $d_b^{-1.5}$ under turbulent conditions. Recently, Gorain et al. (1998) experimentally obtained that the overall flotation rate constant k is strongly correlated with S_b, the average bubble surface area flux in the cell, as

$$k = PS_bR_f \quad (1)$$

where, P is a parameter which represents the mineral floatability and R_f is the froth recovery factor and $S_b = \frac{6Jg}{d_{32}}$ (where Jg is the superficial gas velocity and d_{32} is the Sauter mean bubble diameter). This model has been criticized for being too simplistic, mainly because particle properties were not considered in the model (Heiskanen, 2000).

Although, it is beyond doubt that bubble size is a key parameter in froth flotation, bubble size has rarely been studied in lab scale flotation cells, probably due to the fact that bubble size determination in aerated stirred vessels and particularly in three-phase systems

* Corresponding author. Tel.: +358 9 451 3829; fax: +358 9 451 2795.
E-mail address: rgrau@cc.hut.fi (R.A. Grau).

0892-6875/$ - see front matter © 2005 Elsevier Ltd. All rights reserved.
doi:10.1016/j.mineng.2005.06.011

(solid–liquid–gas) is complex. Tucker et al. (1994) examined the influence of physical and chemical variables on bubble size in a modified 3 dm^3 Leeds flotation cell. Recently, Laskowski et al. (2003) extensively studied the influence of several commercial frothers on bubble size in a 1 dm^3 open-top leads flotation cell. In this study, bubble size was measured using the UCT technique.

Only few investigators have reported measurements of bubble size in industrial cells probably due to the complexity of the measurement and the lack of standard methods to determine it. Jameson and Allum (1984) measured bubble size in operational cells with the use of a photographic technique. They reported that Sauter mean bubble diameters varied over the range of 0.5–1.8 mm. Gorain et al. (1997) reported values measured with the UCT (University of Cape Town) technique, in a 2.8 m^3 portable cell, in the range of 0.7–1.8 mm. While Deglon et al. (2000) using the UCT method found that d_{32} values varied over the range of 1.2–2.7 mm in industrial mechanical cells.

In this project, the influence of operating conditions such as air flow rate, impeller speed and solid concentration on bubble size was investigated, as well as the influence of frother dosage. The objective of this work is to provide a better understanding of the variations in bubble size observed in industrial scale cells. Furthermore, four mathematical distributions are fitted to the experimental data. The purpose of this work is to determine whether bubble size distributions can be satisfactorily represented by a mathematical distribution. The experimental work was carried out in two Outokumpu lab scale flotation cells. The cells were equipped with two rotor–stator designs.

2. Experimental work

The experiments were carried out in two Outokumpu cylindrical flotation cells, a 50 dm^3 laboratory scale cell (35 cm in diameter and 55 cm high) made of stainless steel and a 70 dm^3 cell (42 cm in diameter and 52 cm high) made of plexiglass. In the 50 dm^3 cell (nominal), the level of liquid in the cell was set equal to 35 cm, so a liquid volume of 30 dm^3 was added to cell (Fig. 1). The cell was filled with aqueous solutions of three commercial frothers (Dow Frothers DF-200, DF-250 and DF-1012), which were prepared using municipal tap water. The 50 dm^3 cell is equipped with a multi-mix system and four baffles (from now on referred to as OK-50). The larger cell (from now on referred to as OK-70) was equipped with two rotor–stator combinations: the multi-mix and free-flow mechanisms (Fig. 2). The level of liquid in the OK-70 cell was set equal to the diameter of the cell (42 cm), so a solution volume of 60 dm^3 was initially added to the cell. The OK-70 cell was filled with only aqueous solutions of DF-250.

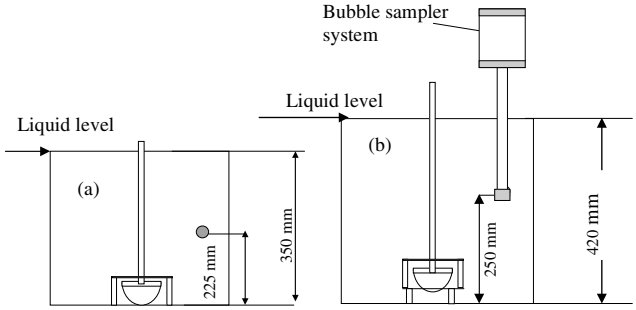

Fig. 1. Sampling location in the (a) OK-50 and (b) OK-70.

Bubble size distributions were determined using the HUT technique (Grau and Heiskanen, 2003). Bubble size was measured at only one location in the cells, above the plane of the stator as shown in Fig. 1. All the experiments were carried out at room temperature (approx. 20 °C). The HUT sampler system (1b) is also filled with aqueous solution of the frothers of the same concentration as the solution in the cell. Each measurement was at least duplicated and on average over 4000 bubbles were sized in each run. The bubble sizes were corrected and they are in this project reported at standard temperature and pressure conditions (25 °C and 1 atm). The correction for temperature and pressure in bubble size determination has been described in detail by Hernandez-Aguilar et al. (2004).

The power input to the OK-70 cell was determined by measuring the torque experienced by the cell as a reaction to the rotating impeller. The cell is supported (mounted) on a thrust bearing, torque table. The torque experienced by the cell is determined with the use of a strain gauge. The power is calculated as follows:

$$P = \frac{T \cdot \pi \cdot N_I}{30} \tag{2}$$

where T is the torque value in N m (N stands for Newton), N_I is the rotational speed of the impeller in rpm and P is the power in N m/s which is equivalent to watt. The impeller speed (N_I) is controlled by a variable speed drive and is measured using a digital tachometer.

2.1. Bubble size distributions

The Rosin–Rammler, Tuniyama–Tanasawa, log-normal and upper-limit distributions were fitted to the experimental data. These four distribution functions have been described in detail elsewhere (Mugele and Evans, 1951; Goering and Smith, 1978; Paloposki, 1994). The experimental data were tabulated and classified in 13 class intervals which were arranged in a geometric progression (with a ratio of $\sqrt{2}$). The adjustable parameters of each mathematical distribution were estimated by a nonlinear least squares fit of the cumulative distribution function to the cumulative bubble volume

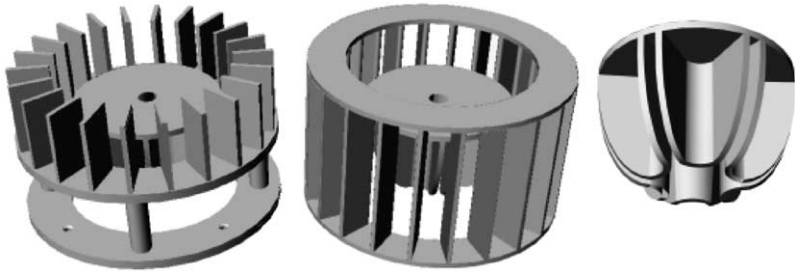

Fig. 2. Rotor/stator mechanisms. From left to right: free-flow mechanism, multi-mix mechanism and OK rotor. Note that both mechanisms use the OK rotor.

distribution. The curve-fitting algorithm was implemented in MATLAB.

3. Results and discussion

Figs. 3 and 4 show graphically the fit of the selected distribution functions to the experimental data obtained from tests conducted in the OK-70 cell. The air flow rate was set at 116 L(STP)/min (1.4 cm/s) and the power consumption in the cell was set at 0.5 kW/m^3. The cell was filled with aqueous solutions of DF-250 at a dosage of 15 ppm. Fig. 3 shows the cumulative bubble volume distribution obtained when the incoming air was dispersed by the free-flow design (OK-FF) and Fig. 4 shows the cumulative bubble volume distribution when the multi-mix mechanism (OK-MM) was used. Over 20,000 bubbles were sized and classified to compute the cumulative bubble volume distributions shown in Figs. 3 and 4.

It is clear from Fig. 3 that the bubble size distribution generated by the free-flow mechanism is satisfactorily described by the upper-limit distribution which is a modification of the log-normal distribution, in fact the

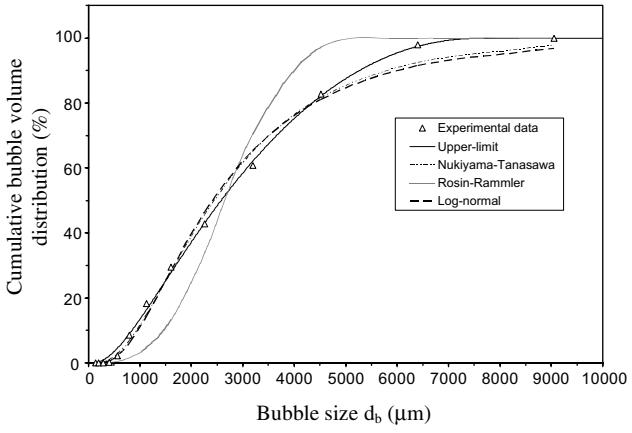

Fig. 3. Nonlinear least square fit of the experimental data obtained from the OK-70 cell equipped with a free-flow mechanism.

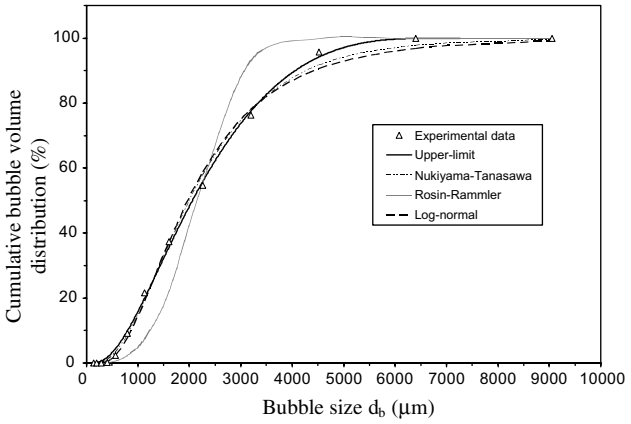

Fig. 4. Nonlinear least square fit of the experimental data collected in the OK-70 cell fitted with the multi-mix mechanism.

upper-limit distribution is also referred to as a three-parameter log-normal distribution. Tavlarides and Stamatoudis (1981) reported that the log-normal distribution appears to be the most common distribution used to describe droplet size distributions in liquid–liquid dispersions. Pacek et al. (1998) suggested that for systems where drop (in this case bubble) break-up occurs as drops break in two, the drop size distribution might be satisfactorily represented by a log-normal distribution. Karabelas (1978) found that drops broken in turbulent liquid–liquid dispersions are satisfactorily represented by the upper-limit distribution.

The bubble volume distribution expressed as the upper-limit distribution is given as (Mugele and Evans, 1951):

$$\frac{\mathrm{d}V}{d_\mathrm{b}} = \frac{\delta}{\sqrt{\pi}} \frac{d_{\mathrm{b\,max}}}{d_\mathrm{b}(d_{\mathrm{b\,max}} - d_\mathrm{b})} \exp\left\{-\delta^2\left[\ln\frac{a d_\mathrm{b}}{d_{\mathrm{b\,max}} - d_\mathrm{b}}\right]\right\}^2 \tag{3}$$

where d_b is the bubble diameter. Integration of Eq. (3) gives the cumulative volume distribution which is presented in Eq. (4) (Goering and Smith, 1978). Note that Eq. (3) is equivalent to the cumulative standard normal distribution.

$$V = \frac{1}{\sqrt{\pi}} \int_{-\infty}^{\delta z} \exp(-u)^2 \, du \tag{4}$$

where z is defined as

$$z = \ln \frac{a d_b}{d_{b\,max} - d_b} \tag{5}$$

As can be seen from Eqs. (3) and (4), three parameters are required to specify the upper-limit distribution: $d_{b\,max}$ is the hypothetical maximum bubble diameter in the distribution, a is a dimensionless parameter and δ is a dimensionless parameter related to the geometric standard deviation. When these three parameters are known, the Sauter mean bubble diameter can be determined from the bubble size distribution equation (Mugele and Evans, 1951):

$$d_{32} = \frac{d_{b\,max}}{1 + a \cdot \exp\left(\frac{1}{4\delta^2}\right)} \tag{6}$$

The upper-limit distribution also provided a good fit of the experimental data obtained from the tests conducted in the OK-70 cell equipped with the multi-mix mechanism, as can be seen from Fig. 4. It also clear from Figs. 3 and 4 that the log-normal, Nukiyama–Tanasawa and specially the Rosin–Rammler distribution provided a poor fit to the experimental data. The same trend was also evident when these four mathematical models were fitted to experimental data obtained at different operating conditions in the OK-50 cell. Table 1 summarizes the upper-limit distribution parameters obtained through curve fitting. Sauter mean diameter values (d_{32}) computed directly by summation of the data and from Eq. (6) are also listed in Table 1.

The Sauter mean diameter or surface-volume mean diameter d_{32} is usually the most relevant average in cases where the interfacial area is a control parameter. Jameson and Allum (1984) suggested that the Sauter mean diameter is the appropriate average bubble diameter to represent bubble size distributions in flotation machines. Lately, several authors have adopted the Sauter mean diameter to describe bubble size distributions (gas dispersion conditions) in flotation cells and columns. Therefore, the good agreement found between the Sauter mean diameters calculated directly from the experimental data and from Eq. (6) (Table 1), reinforces the argument that the upper-limit distribution can be used to represent bubble size distributions. In addition, the quality of the fit of the upper-limit function to the experimental data is shown graphically in Figs. 6, 8, 11, 13, 14 and 16.

3.1. Effect of frothers on bubble size

The experimental work using the OK-50 cell was conducted with three commercial Dow frothers: DF-200, DF-250 and DF-1012. The impeller speed was set at 1050 rpm (tip speed: 6.9 m/s) and the air flow rate was set at 77 dm^3 (STP)/min (superficial gas velocity $Jg = 1.3$ cm/s). The results of the measurements are shown graphically in the form of bubble size vs. frother concentration curves in Fig. 5.

As can be seen from Fig. 5, the general trend for all the investigated frothers was fairly similar, the bubble size decreased with increasing frother dosage, and at a particular concentration, the bubble size levelled off. Cho and Laskowski (2002) suggested that frothers control bubble size by reducing bubble coalescence in the cell and that coalescence is entirely prevented at concentrations exceeding the critical coalescence concentration (CCC) in a dynamic system. It is clear from Fig. 5 that

Table 1
Parameters of the fitted upper-limit distribution

Cell rotor/stator	Jg (cm/s)	Impeller speed (rpm)	a	δ	$d_{b\,max}$ (mm)	d_{32} (Eq. (6)) (mm)	d_{32} (data) (mm)
OK-50[a] multi-mix	0.7	350	1.62	0.96	9.69	3.15	2.92
		450	1.42	0.85	6.35	2.11	1.97
		550	1.72	0.75	6.47	1.76	1.66
		650	1.79	0.74	6.16	1.73	1.56
		750	2.19	0.76	6.63	1.51	1.49
		850	2.74	0.73	6.50	1.20	1.31
		950	2.74	0.73	6.50	1.20	1.26
		1050	2.57	0.69	6.20	1.16	1.21
		1100	3.20	0.73	6.90	1.12	1.20
OK-50 multi-mix 10% solids	0.7	1050	3.6	0.84	7.31	1.19	1.26
OK-50 multi-mix 30% solids	0.7	1050	1.4	0.69	6.04	1.76	1.74
OK-70[a] multi-mix	1.4	700	2.5	0.78	7.28	1.51	1.54
OK-70[a] free-flow	1.4	660	2.1	0.65	8.03	1.67	1.74

[a] The tests were conducted with only aqueous solutions of the frothers.

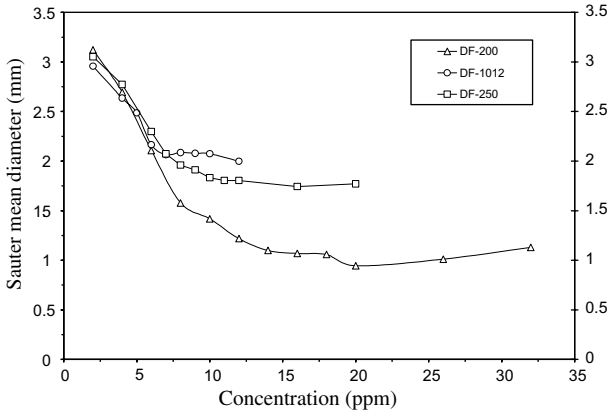

Fig. 5. Effect of frothers concentration on bubble size (OK-50).

the CCC value is different for each type of frother. At frother dosages exceeding the CCC value, the conditions in the cell can be defined as non-coalescing.

Fig. 6 shows the bubble volume distributions measured at frother dosages exceeding the CCC values. It is clear from Figs. 5 and 6 that at frother concentrations exceeding the CCC values, different bubble sizes were observed. Thus, it can be mentioned that the DF-200 was the most effective frother in terms of bubble size reduction and the least effective was DF-1012. These results suggest that frothers do not only hinder coalescence but also somehow affect bubble break-up under turbulent conditions, and this effect appears not to be directly related to the surface tension of the solution.

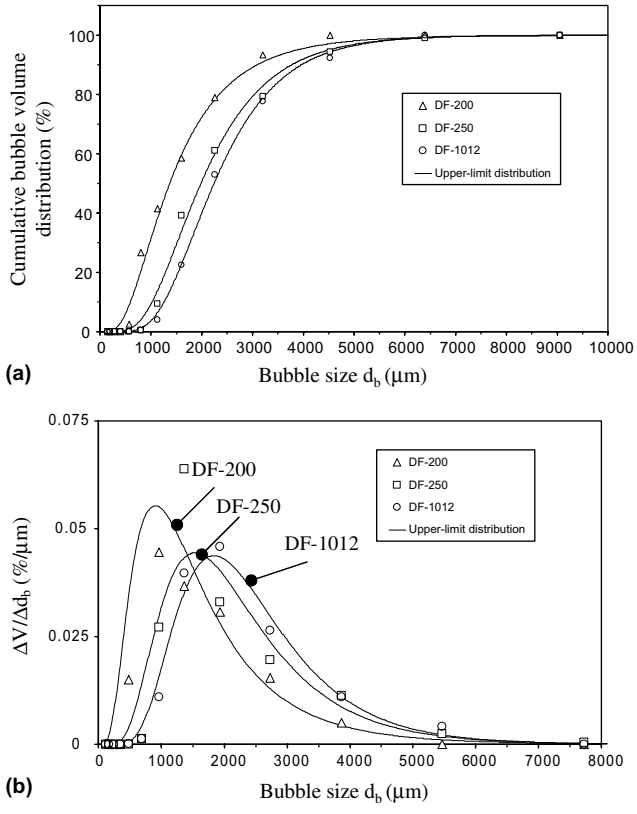

Fig. 6. Bubble size distribution measured at concentrations exceeding the CCC values for three different frothers: (a) cumulative size distribution represented by an upper-limit distribution and (b) frequency plots of bubble volume presented as continuous curves using the fitted upper-limit functions.

3.2. Effect of impeller tip speed

Sauter mean bubble diameter is plotted against impeller speed at different air rates in Fig. 7. The impeller speed in the OK-50 cell was varied between 1.64 and 7.2 m/s (250–1100 rpm). The air flow rate was set at two levels during the experiments, in terms of superficial gas velocity, 0.7 cm/s (STP) and 1.3 cm/s (STP). Fig. 7 also includes mean bubble sizes obtained from tests carried out in the OK-70 cell. Fig. 7 allows us to compare the gas dispersion conditions achieved in each cell. In order to establish non-coalescing conditions in the experiments, DF-250 was used at a dosage of 15 ppm. This concentration exceeds the CCC value of this particular frother, which was found to be 9.1 ppm (or 0.035 mmol/dm^3). The CCC value determination has been explained in detail by Laskowski et al. (2003).

It is clear from Fig. 7 that the Sauter mean bubble diameter in the OK-50 cell decreased continuously with increasing impeller tip speed. The same kind of trend has also been observed in stirred vessels (Parthasarathy et al., 1991). Takahashi et al. (1992) measured bubble size in a vessel agitated by a Rushton turbine using a photographic technique. At very low aeration conditions in the vessel, they observed that the Sauter mean diameter at locations very close to the impeller, near the aerated cavities (vortex cavities), varies as $N_I^{-0.5}$, where N_I is the rotational speed of the impeller. Machon et al. (1997) gave the following relationship between Sauter mean diameter (d_{32}) and impeller speed:

$$d_{32} \propto N_I^{-\beta} \tag{7}$$

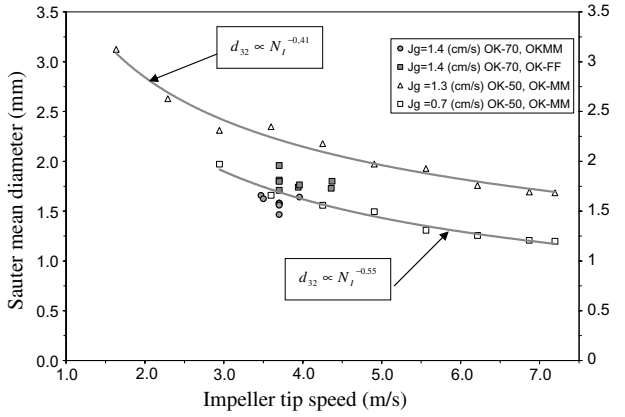

Fig. 7. Effect of impeller tip speed upon bubble size. OK-MM refers to the multi-mix design and OK-FF to the free-flow design.

where $0.34 < \beta < 0.61$. In spite of the differences in the experimental operating conditions, the β values derived from the experimental data shown in Fig. 7, agree very well with the values given by Machon et al. (1997). In the larger cell (OK-70), no clear trend was observed between the bubble size and impeller speed, probably due to the narrow range of impeller speeds tested.

In terms of bubble generation, it is clear from Fig. 7 that the OK-70 cell was capable of producing finer bubbles sizes even at higher air rates (see Fig. 12). An explanation of the difference observed in bubble size can probably be found in the cell geometries. The OK-50 cell is fitted with four equidistant vertical baffles, while the OK-70 cell does not contain any baffle. The baffles might dampen the turbulent intensity in the cell.

As can be seen from Figs. 8 and 9, the amount of fine bubbles increased as the impeller tip speed increased. Intense agitation combined with fine bubbles improves the attachment process. However, intense agitation could be detrimental to flotation, owing to particle detachment (Deglon et al., 1999).

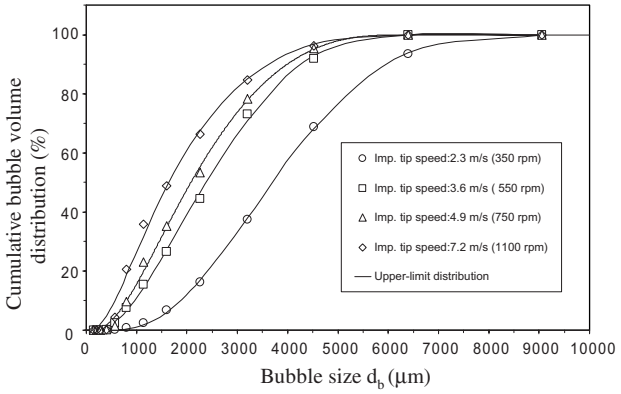

Fig. 8. Effect of the impeller speed on cumulative bubble volume distribution. The solid lines correspond to the fitted upper-limit distribution (OK-50).

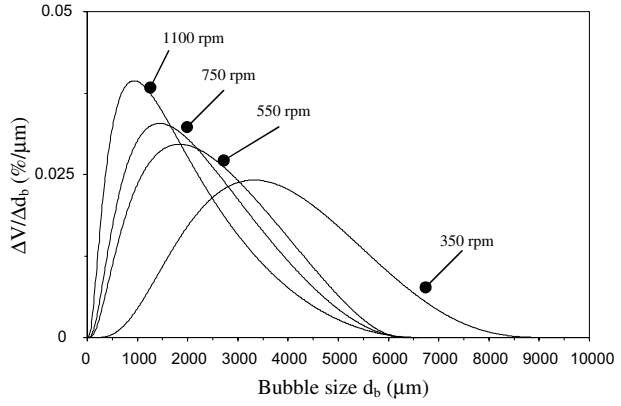

Fig. 9. Fitted upper-limit distributions at different impeller speeds (OK-50).

3.3. Effect of rotor–stator mechanism on bubble generation

Fig. 10 shows the results of the bubble size measurements conducted in the OK-70 cell. Two set of rotor–stator mechanisms were used for the experimental work in the 70 dm^3 cell, the multi-mix mechanism (OK-MM) and free-flow mechanism (OK-FF). The rotor–stator designs are shown in Fig. 2. The power input to the cell was kept constant at 0.5 kW/m^3 (power input per unit volume) by altering the impeller speed at constant air rate.

As can be seen in Fig. 10, the multi-mix design appears to produce slightly finer bubbles than the second mechanism. The variations in bubble size are also illustrated in Fig. 11. These differences appear to be related to the specific function of the mechanisms. The multi-mix mechanism is the general-purpose design, which is commonly used to treat fine and medium range particle sizes. The free-flow mechanism is designed primarily for coarser particle flotation. With this mechanism excessive turbulence is avoided in order to reduce particle detachment. It is clear from Fig. 11 that the free-flow mechanism produces bubbles of a wider size range. Broad bubble size distributions might have a positive effect on the flotation of coarse particles. According to Tao (2004), the presence of larger bubbles strengthens the levitation of coarse particles (bubble–particle aggregate).

3.4. Effect of air flow rate

The effect of superficial gas velocity on bubble size is shown graphically in Figs. 12–14. As can be seen in Fig. 12, bubble size increased with increasing air flow rate. It was found that the bubble-size distribution was shifted towards larger bubble size as the air rate was increased (Fig. 14). It was also observed that the width of the distribution increased with increasing air flow rate over the range of air rates investigated. These measurements were also conducted in what can be considered

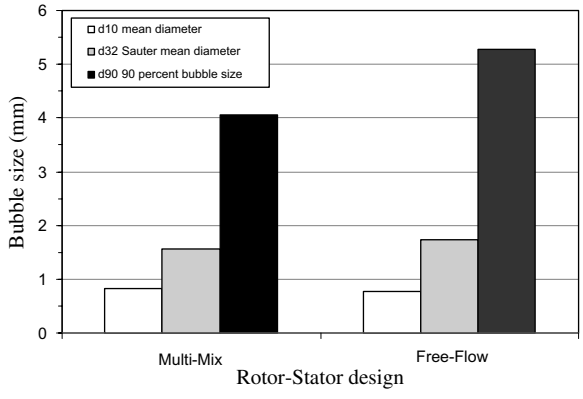

Fig. 10. Bubble size measured using two rotor–stator combinations (OK-70), d_{90} was calculated graphically from Fig. 11.

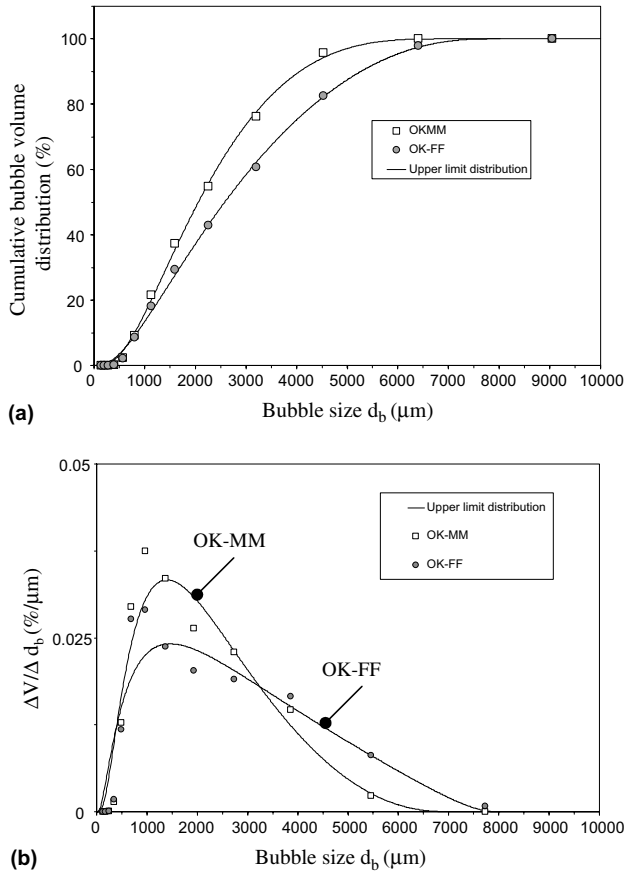

Fig. 11. Bubble size distributions generated by two different rotor–stator mechanisms: (a) cumulative size distribution represented by an upper-limit distribution and (b) comparison of experimental data with the fitted upper-limit distributions (OK-70).

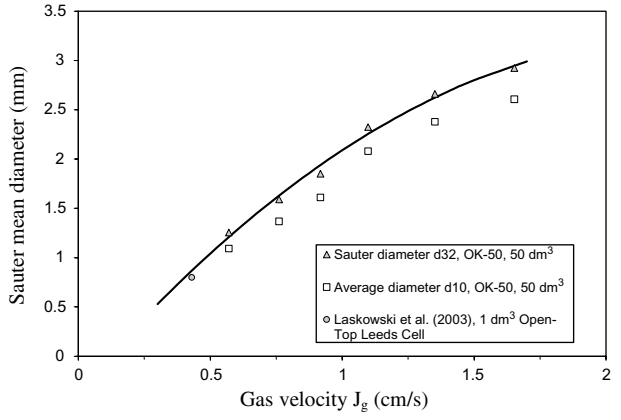

Fig. 12. Effect of air flow rate on bubble size. DF-250, 10 ppm and impeller speed 800 rpm (Grau and Heiskanen, 2003).

non-coalescing conditions. Fig. 12 also includes experimental data published by Laskowski et al. (2003) at similar operating conditions.

The influence of the air flow rate (or gas velocity) on bubble size is intrinsically related to presence of air cavities behind the blades of the rotor. The presence of air

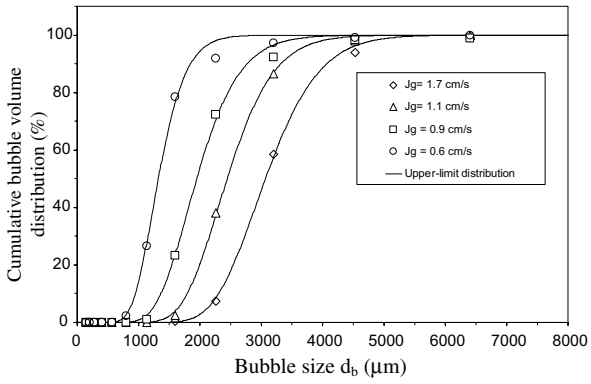

Fig. 13. Cumulative bubble volume distribution in a mechanical cell at different air rates (OK-50).

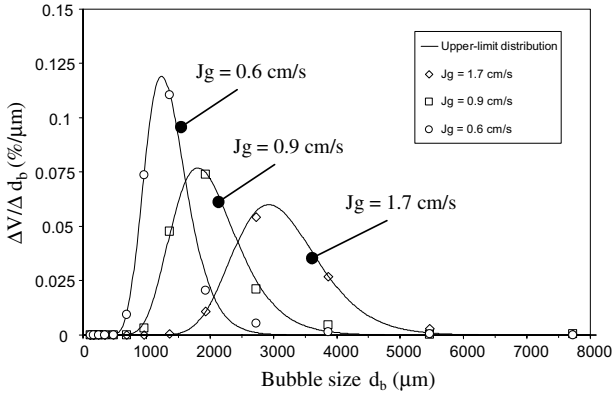

Fig. 14. Influence of the air flow rate on bubble size distribution, comparison of experimental data with the fitted distributions (OK-50).

cavities and their size affect the power consumption in the cell. Grainer-Allen (1970) observed that as air is introduced into the flotation cell, the air collects behind the blades of the rotor forming air cavities. Bruijn et al. (1974) observed that in aerated vessels with Rushton turbines, these air cavities enlarge as the gas flow rate increases, causing the power requirement to continuously diminish. Parthasarathy et al. (1991) found that the maximum stable bubble size, in non-coalescing conditions, varies as $[\frac{P}{V}]^{-2/5}$, where P is the power consumption and V is the impeller swept volume.

3.5. Effect of a non-floatable solid

The material selected for the experimental work was quartz ($d_{50} = 160$ mm). The tests were conducted in the OK-50 without collector, therefore, the solid can be classified as a non-floatable solid. The air flow rate in the cell was set at 38 dm^3 (STP)/min ($Jg = 0.7$ cm/s) and the impeller speed was set at 1050 rpm. The solid concentration was varied over the range of 0–30% (kg/kg) using two frothers, DF-250 and DF-1012, at concentrations of 15 ppm and 10 ppm, respectively. The frother

concentrations were selected in order to establish non-coalescing conditions in the cell. The measurements consisted of two runs, on average over 7000 bubbles were sized in each run.

The effect of the non-floatable solid concentration on the mean bubble size is shown graphically in Figs. 15 and 16.

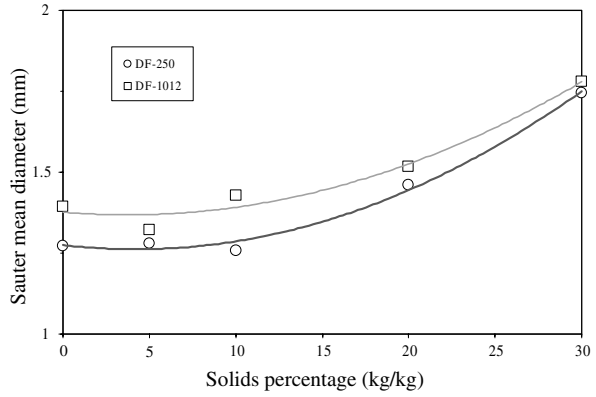

Fig. 15. Effect of a non-floatable solid upon bubble size (OK-50).

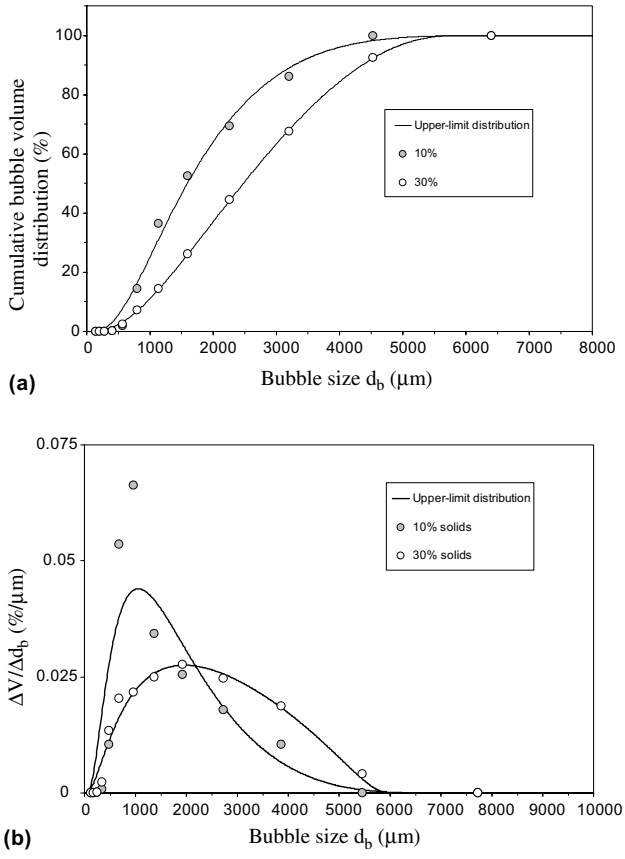

Fig. 16. Bubble size distribution at two solids concentrations: (a) cumulative size distribution represented by an upper-limit distribution and (b) comparison of experimental data with the fitted distributions (OK-50).

It is clear from Fig. 15 that the Sauter mean bubble diameter increased with the addition of quartz, independent of the type of frother used. The influence of the particles in the pulp was found to be stronger at concentrations exceeding 20% (kg/kg). It was also found that DF-250 produced smaller sizes of bubbles than the second frother over the range of operating conditions investigated. Similar findings on the effect of solids concentration have been reported by Tucker et al. (1994).

It seems that the presence of solids dampens the turbulent intensity in the cell, which produces an increase in the amount of bubbles in the larger classes, as is illustrated in Fig. 16. The increase in solid concentration has a strong influence on the apparent density and viscosity of the suspension.

4. Conclusions

1. The experimental data obtained from the tests conducted in two lab scale flotation cells was well represented by the upper-limit distribution. The Sauter mean diameter values computed from the experimental data, showed a good agreement with the values calculated from the fitted cumulative bubble volume distributions.
2. It seems that frothers mainly control bubble size in flotation cell by decreasing coalescence and that coalescence is completely hindered at frother dosages exceeding the CCC value. Non-coalescing conditions in a flotation cell can therefore be established using frothers at dosages exceeding the CCC values. The CCC value seems to be different for each type of frother. It was found that with increasing frother concentration, bubble size decreased until the CCC value is reached. At concentrations above CCC, no further changes in bubble size were observed.
3. The air flow rate was found to have a profound impact on bubble size. The Sauter mean bubble diameter increased with increasing air rate over the range of operating conditions investigated.
4. The impeller speed was found to have an important effect on bubble size, the mean bubble size (d_{32}) decreased as the impeller speed increased.
5. With the addition of quartz, the mean bubble size was found to increase. The influence of the solid concentration on bubble was more evident at concentrations exceeding 20% (kg/kg).

References

Ahmed, N., Jameson, G., 1985. The effect of bubble size on the rate of flotation of fine particles. International Journal of Mineral Processing 14 (3), 195–215.

Bruijn, W., Van't Riet, K., Smith, J.M., 1974. Power consumption with aerated Rushton turbines. Trans. Inst. Chem. Engrs 52, 88–104.

Cho, Y.S., Laskowski, J.S., 2002. Effect of flotation frothers on bubble size and foam stability. International Journal of Mineral Processing 64 (2–3), 69–80.

Deglon, D.A., Egya-Mensah, D., Franzidis, J.P., 2000. Review of hydrodynamics and gas dispersion in flotation cells on South African platinum concentrators. Minerals Engineering 13 (3), 235–244.

Deglon, D., Sawyerr, F., O'Connor, C., 1999. A model to relate the flotation rate constant and the bubble surface area flux in mechanical flotation cells. Minerals Engineering 12 (6), 599–608.

Goering, C., Smith, D., 1978. Equations for droplet size distributions in sprays. Transactions of the Asae 21 (2), 209–216.

Gorain, B., Franzidis, J., Manlapig, E., 1997. Studies on impeller type, impeller speed and air flow rate in an industrial scale flotation cell. Part 4: effect of bubble surface area flux on flotation performance. Minerals Engineering 10 (4), 367–379.

Gorain, B., Franzidis, J., Manlapig, E., 1998. Studies on impeller type, impeller speed and air flow rate in an industrial scale flotation cell. Part 5: validation of k-Sb relationship and effect of froth depth. Minerals Engineering 11 (7), 615–626.

Grainer-Allen, T.J., 1970. Bubble generation in froth flotation machines. Transactions of the Institution of Mining and Metallurgy Section C 79, C15–C22.

Grau, R., Heiskanen, K., 2003. Gas dispersion measurements in a Flotation cell. Minerals Engineering 16 (11), 1081–1089.

Jameson, G., Allum, P., 1984. A survey of bubble sizes in industrial flotation cells, report prepared for AMIRA limited.

Heiskanen, K., 2000. On the relationship between flotation rate and bubble surface area flux. Minerals Engineering 13 (2), 141–149.

Hernandez-Aguilar, J., Coleman, R., Gomez, C., Finch, J., 2004. A comparison between capillary and imaging techniques for sizing bubbles in flotation systems. Minerals Engineering 17 (1), 53–61.

Karabelas, A., 1978. Droplet size spectra generated in turbulent pipe flow of dilute liquid/liquid dispersions. AIChE Journal 24 (2), 170–180.

Laskowski, J.S., Tlhone, T., Williams, P., Ding, K., 2003. Fundamental properties of the polyoxypropylene alkyl ether flotation frothers. International Journal of Mineral Processing 72 (1–4), 289–299.

Machon, V., Pacek, A.W., Nienow, A.W., 1997. Bubble size in electrolyte and alcohol solutions in a turbulent stirred vessel. Transactions IChemE 75, 339–348.

Mugele, R., Evans, H., 1951. Droplet size distributions in sprays. Industrial and Engineering Chemistry 43 (6), 1317–1324.

Pacek, A., Man, C., Nienow, A., 1998. On the Sauter mean diameter and size distributions in turbulent liquid/liquid dispersions in a stirred vessel. Chemical Engineering Science 53 (11), 2005–2011.

Paloposki, T., 1994. Drop size distributions in liquid sprays. Acta Polytechnica Scandinavica, Mechanical Engineering series 114.

Parthasarathy, R., Jameson, G.J., Ahmed, N., 1991. Bubble breakup in stirred vessels—Predicting the Sauter mean diameter. Transactions IChemE 69, 295–301.

Takahashi, K., McManamey, W.J., Nienow, A.W., 1992. Bubble size distributions in impeller region in a gas sparged vessel by a Rushton turbine. Journal of Chemical Engineering of Japan 25, 427–432.

Tao, D., 2004. Role of bubble size in flotation of coarse and fine particles—a review. Separation Science and Technology 39 (4), 741–760.

Tavlarides, L., Stamatoudis, M., 1981. The analysis of interphase reactions and mass transfer in liquid–liquid dispersions. Advances in Chemical Engineering 11, 199–273.

Tucker, J.P., Deglon, D.A, Franzidis, J.P., Harris, M.C., O'Connor, C.T., 1994. An evaluation of a direct method of bubble size distribution measurement in a laboratory batch flotation cell. Minerals Engineering 7 (5–6), 667–680.

Yoon, R., 2000. The role of hydrodynamic and surface forces in bubble particle interaction. International Journal of Mineral Processing 58 (1–4), 129–143.